J. Fluid Mech. (1986), *vol.* 170, *pp.* 233–252
Printed in Great Britain

Experimental study of secondary flow in a magnetohydrodynamic channel

By S. L. GIRSHICK† AND C. H. KRUGER
Department of Mechanical Engineering, Stanford University, Stanford, CA 94305, USA

(Received 12 August 1985 and in revised form 3 March 1986)

The Hall effect in the magnetohydrodynamic (MHD) channel flow of a plasma leads to the presence of transverse Lorentz forces. The non-uniform distribution of these body forces may cause secondary flows to develop; these can exert a significant influence on the plasma momentum, thermal and electrical behaviour. The effect is predicted to be large for envisioned large-scale MHD devices. An experimental study of this phenomenon is described. The apparatus consisted of a laboratory-scale MHD channel in which a controlled net axial current was applied. Plasma velocities were measured using laser-Doppler anemometry. The results demonstrate that transverse Lorentz forces can drive intense secondary flows at a value of the magnetic interaction parameter based on the Hall current of approximately one. The peak measured transverse velocities were 15 % of the bulk velocity. Qualitatively, the basic character of the large-scale secondary flow structure was in accord with a simple model based on a first-order distribution of the axial current density. Measurements were also made under a variety of conditions of the profiles of mean axial velocity and of the axial and transverse components of turbulence intensity, of electrode surface temperatures and of plasma voltage distributions. These results all support the conclusion that convective transport by MHD secondary flow caused significant asymmetries to develop in the cross-plane distribution of scalar quantities.

1. Introduction

The channel flow of a plasma through a transverse magnetic field is influenced by the Hall effect, which causes non-uniform Lorentz forces to arise in the direction mutually perpendicular to the channel axis and the magnetic field. These forces cause secondary flows to develop as the flow progresses down the region of electromagnetic–fluid interaction. The theoretical treatment of this problem has included the work of Fay (1959), Broer, Peletier & Wijngaarden (1960), Sato (1961), Tani (1962), Apollonskii & Kos'kin (1968), Sastry & Bhadram (1978), Liu, Lineberry & Schmidt (1983) and Ishikawa & Umoto (1984); in particular, for conditions that would be typical of a commercial-scale MHD power generator, these secondary flows were predicted to be of substantial magnitude in the calculations reported by Maxwell *et al.* (1977), Bityurin, Zatelepin & Lyubimov (1978) and Doss & Ahluwalia (1983). The calculated magnitude of these flows for a commercial-scale device ranges from 10–30 % of the bulk velocity, depending on conditions, and the predicted consequences include the development of significant asymmetries in the profiles of mean axial velocity and of temperature, with resultant effects on wall heat transfer and electrode

† Present address: Department of Mechanical Engineering, University of Minnesota, 111 Church Street Southeast, Minneapolis, MN 55455 USA.

voltage drops. In addition Demetriades *et al.* (1981) predicted that these secondary flows could lead to magnetoaerothermal instabilities, which could include boundary-layer separation and/or electric-field breakdown near the electrodes.

Indirect evidence for the existence of MHD-induced secondary flow, reviewed by Girshick & Kruger (1983), included measurements of temperature profiles obtained by James & Kruger (1983) and of electrode voltage drops obtained by Barton (1980), which indicated that MHD effects caused the anode (top) wall boundary layer of the channel to be colder than expected while the cathode (bottom) wall was hotter than expected. It was hypothesized that these results could be ascribed to a secondary-flow mechanism. Demetriades *et al.* (1983) conjectured that evident arc damage to the centre of the anode wall in the downstream half of the channel used in the High Performance Demonstration Experiment at the Arnold Engineering Development Center (Starr *et al.* 1982) was a manifestation of the magnetoaerothermal instability mentioned above. McClaine, Swallom & Kessler (1985) reported axial velocity profiles measured using a traversing stagnation pressure probe mounted in the diffuser of the Avco Mk VI generator. The profile measured between the top and bottom walls was found to be strongly skewed by MHD forces, presumably as a consequence of secondary flow.

The work reported in the present paper consisted of experiments in which the first direct, quantitative measurements of the secondary-flow field in an MHD channel were obtained. Additionally the effect of secondary flow on the plasma momentum, thermal and electrical behaviour was studied by making measurements of the profiles of mean axial velocity, turbulence intensity (axial and transverse) and plasma voltage, and by measuring electrode surface temperatures.

These experiments were performed under conditions that were not ideal, in that the flow in a combustion-driven MHD channel is inherently less 'clean' than in a carefully arranged laboratory flow involving low-temperature air or water. Factors such as combustion non-uniformities, cooled walls, and irregularities in the electrode–insulator wall structure inevitably affect the flow. Nevertheless, the present experiments were designed so as to minimize extraneous effects to the extent possible. Also, the channel was run under non-slagging conditions, and the measurements were made under different orientations of the magnetic field, and with the magnet turned off, so as to isolate the effects on the flow field of Lorentz forces as opposed to non-ideal conditions.

2. Theoretical background

We consider the geometry pictured in figure 1. The channel is a rectilinear duct whose axis points in the x-direction. An external magnet supplies a uniform magnetic induction $\boldsymbol{B}$, pointing in the z-direction. The magnetic Reynolds number being assumed small, the induced magnetic field is negligible in comparison with the applied field.

Through the channel flows a potassium-seeded combustion plasma characterized by velocity $|\boldsymbol{u}| \sim 100$–$1000$ m/s, temperature $T \sim 2700$ K, pressure $P \sim 1$ atm, scalar electrical conductivity $\sigma \sim 10$ S/m and electron mobility $\mu_e \sim 0.4$ m^2/(V s). For an applied induction of ~ 2.5 T the electron Hall parameter β has a value of ~ 1.

The motion of charged particles through the magnetic field establishes a $\boldsymbol{u} \times \boldsymbol{B}$ Faraday field (in the laboratory frame of reference) which points in the y-direction. In an MHD generator this field is utilized by drawing current through electrodes placed in the top and bottom walls, these electrodes being connected through an

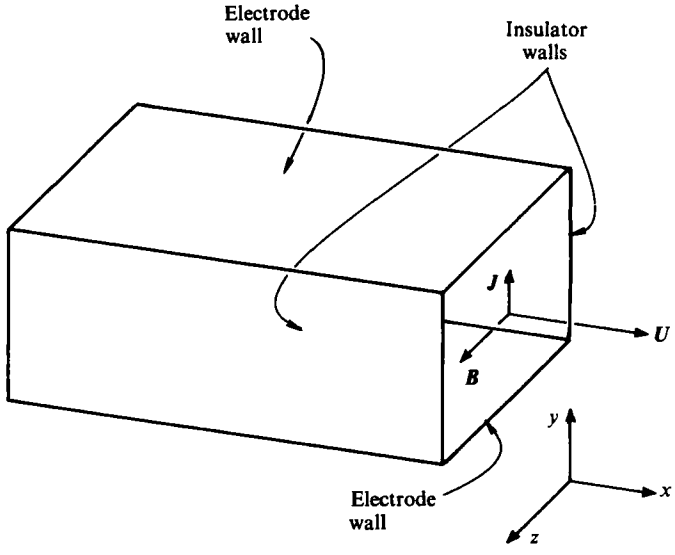

FIGURE 1. Schematic representation of an MHD channel.

external load. In addition to the Faraday current J_y, the Hall effect for a partially ionized gas causes the current density vector $\boldsymbol{J}$ to have a local component in the x-direction. This can be expressed by considering the conductivity as a tensor and writing Ohm's Law in the form (see e.g. Mitchner & Kruger 1973)

$$\boldsymbol{J} = \boldsymbol{\sigma}\boldsymbol{E}', \tag{1}$$

where $\boldsymbol{E}'$ is the electric field in a frame of reference moving with the mean mass velocity of the fluid and, assuming ion slip to be negligible,

$$\boldsymbol{\sigma} = \frac{\sigma}{1+\beta^2}\begin{bmatrix} 1 & -\beta & 0 \\ \beta & 1 & 0 \\ 0 & 0 & 1 \end{bmatrix}. \tag{2}$$

For simplicity let us suppose that the Hall current J_x is everywhere non-negative, as pictured in figure 2. In a combustion MHD channel the walls must be cooled because of materials constraints, and consequently the plasma is much more conductive in the core than near the walls. Furthermore the $\boldsymbol{u}\times\boldsymbol{B}$ interaction goes to zero at the walls because of the no-slip condition. Thus to first order the profile $J_x(z)$ would appear approximately as indicated in figure 2.

The fluid momentum equation under the stated conditions can be written

$$\rho\frac{\mathrm{D}\boldsymbol{u}}{\mathrm{D}t} = -\nabla p + \nabla\boldsymbol{\tau} + \boldsymbol{J}\times\boldsymbol{B}, \tag{3}$$

where ρ is the mass density, p the thermodynamic pressure and $\boldsymbol{\tau}$ the viscous stress tensor. With $\boldsymbol{B} = (0, 0, B_z)$ the presence of a non-zero Hall current causes the $\boldsymbol{J}\times\boldsymbol{B}$ Lorentz force to have a component in the y-direction. Taking the curl of (3) to obtain the fluid vorticity equation, we obtain for the vorticity $\boldsymbol{\Omega}$ the result

$$\rho\frac{\mathrm{D}\boldsymbol{\Omega}}{\mathrm{D}t} = \nabla\times(\boldsymbol{J}\times\boldsymbol{B}) + (\text{viscous terms}) + (\text{density-gradient terms}). \tag{4}$$

In a combustion-driven MHD channel the flow is generally turbulent, so that the viscous terms are dominated by Reynolds stresses. Moreover, the density is non-

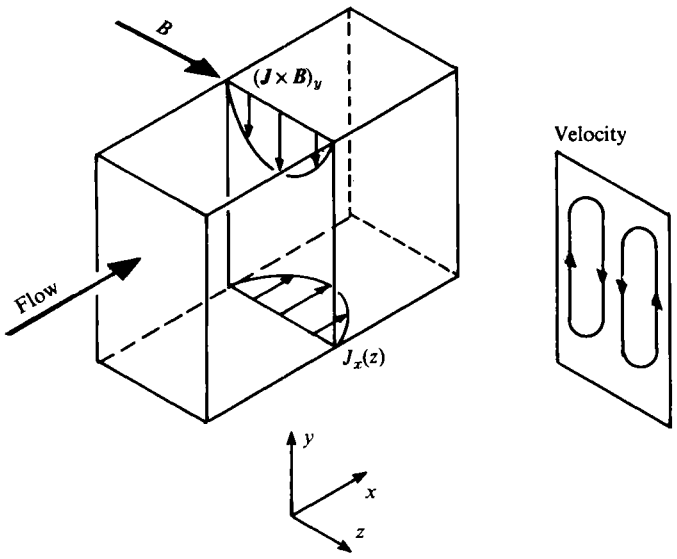

FIGURE 2. Secondary-flow mechanism for a case of positive net Hall current.

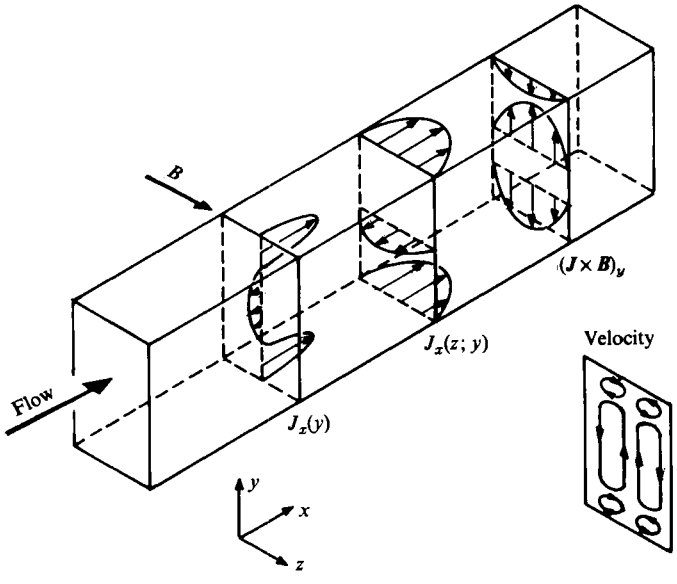

FIGURE 3. Secondary-flow mechanism for a segmented Faraday generator (zero net Hall current).

uniform because the walls are cooled. Neglecting these effects and assuming that B_z = constant we obtain the following expression for the contribution of Lorentz forces to the axial vorticity component:

$$\rho \frac{\mathrm{D}\Omega_x}{\mathrm{D}t} = B \frac{\partial J_x}{\partial z}. \tag{5}$$

It is thus evident that the non-uniformity of the Hall current density between the core and the sidewalls introduces a rotational component into the Lorentz force. For

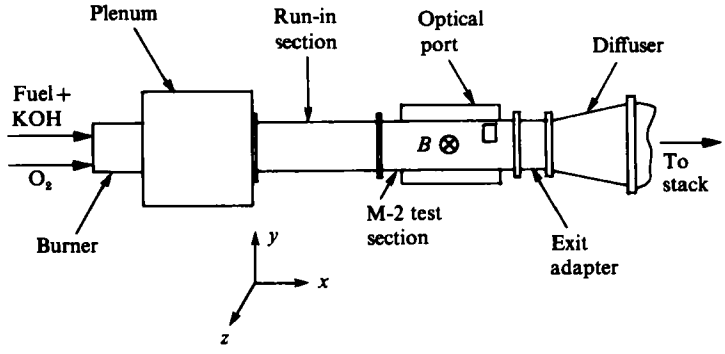

FIGURE 4. M-2 flow train.

the first-order profile of J_x pictured we would expect the two-cell flow structure shown on the right of figure 2 to arise. The presumed effect of such a secondary flow would be to transport hot, fast core plasma towards the bottom wall while sweeping relatively cold, slow sidewall fluid into the boundary layer of the top wall.

As the axial vorticity and the distribution of J_x are coupled through (5), the actual structure of the secondary flow field could be considerably more complicated than the simple pattern suggested in figure 2; indeed, J_x might not increase monotonically from the walls to the core, in which case the axial vorticity could change sign in some regions of the cross-plane. It should also be pointed out that commercial Faraday MHD generators would suppress the flow of net Hall current by using segmented electrodes separated by insulators. However, the Hall effect would still cause the local value of J_x to be in general non-zero; only the integrated value of J_x over the cross-plane would vanish, and then only in the absence of axial leakage currents. A typical profile of J_x under these circumstances and of the resulting six-cell secondary-flow field are shown in figure 3. For the conditions of envisioned commercial-scale MHD generators the strength of these secondary flows could be significant, in spite of the suppression of net Hall current; this case was discussed by Swean *et al.* (1981) as well as by several of the authors cited earlier.

3. Description of experiments

3.1. *Flow train and run conditions*

MHD secondary flow was investigated in a series of experiments conducted at the High Temperature Gasdynamics Laboratory at Stanford University. The M-2 flow train, shown in figure 4, was used. This consisted of a combustor with a nominal 2 MW thermal input rating, a large mixing plenum, a nozzle through which the combustion products were accelerated into a duct having a square cross-section measuring 5.1 cm on a side, a diffuser and an exhaust system including a scrubber and a stack. The square duct consisted of a run-in section, and the active channel itself, which was enclosed in a 2.6 T water-cooled copper-coil magnet. Physical dimensions of the flow train are given in table 1, including distances from the nozzle exit to the measurement locations.

Run conditions are listed in table 2. The plasma consisted of the combustion products of ethanol burned in pure oxygen. The fuel was seeded with potassium hydroxide. The total flow rate, 54.4 g/s, at a calculated nozzle exit temperature of

Component	Dimensions (cm)
Combustor	$D = 8.9$, $L = 36.8$
Plenum	$H = 22.9$, $W = 17.8$, $L = 48.3$
Nozzle	$H = W = 5.08$, $L = 2.5$
Run-in section	$H = W = 5.08$, $L = 50.8$
Active channel	$H = W = 5.08$, $L = 74.9$
Extender section	$H = W = 5.08$, $L = 20.3$
Diffuser	$H = 13.3$, $W = 6.4$ expanding to 13.3, $L = 43.2$
Transfer tube	$D = 25.4$, $L = 290$
Vertical exhaust/scrubber system	

Distances from nozzle exit (cm)	
Active channel entrance	50.8
Centre of first electrode	64.1
Conductivity measurement plane	98.4
Temperature measurement plane	102.2
Velocity measurement plane	108.9 (21.4 hydraulic diameters)
Centre of last electrode	109.9

Electrodes: $W = 5.08$ cm, $L = 1.91$ cm.

D, diameter; H, height; W, width; L, length

TABLE 1. Channel geometry.

2750 K, corresponded to a Reynolds number (based on hydraulic diameter) of 1.3×10^4; the calculated nozzle exit velocity was 171 m/s. This value has been used throughout to characterize the bulk velocity U_b, although it should be noted that the actual bulk velocity decreases somewhat in the downstream direction as the plasma cools. The flow thus being turbulent, the boundary layers at the velocity measurement plane, which was 21.4 hydraulic diameters downstream of the nozzle exit, were fully developed (or at least nearly so) in the absence of MHD interaction.

3.2. *Electrical configuration*

An important goal of the experiments was to isolate the effect on the fluid flow of the Hall current, since the Faraday current itself has important effects because it induces an axial Lorentz force given by $J_y B$. It was also considered desirable to establish conditions that allowed as far as possible a straightforward interpretation of the measured secondary flow field. Accordingly the channel was connected in the 'Hall configuration', with a pair of electrodes at the upstream end connected through an external load to a pair of electrodes at the downstream end, as shown in figure 5. A controlled current of 9.3 A was driven through the plasma by means of a bank of batteries, and by varying the load resistance. Thus the experimental situation corresponded to the case illustrated in figure 2, with a positive net Hall current.

A non-dimensional parameter that indicates the strength of the electromagnetic–fluid interaction is the Stuart number, or magnetic interaction parameter, S. For this configuration an appropriate definition of S is

$$S \equiv \frac{I_x BL}{\dot{m}U}, \tag{6}$$

where I_x is the applied Hall current, L the distance from the first loaded electrode to the measurement plane, $\dot{m}$ the mass flow rate and U the mean axial velocity. The interaction parameter in this form represents the ratio of the Lorentz twisting force

Fuel	Ethyl alcohol (C_2H_5OH)
N_2/O_2 ratio	0
Stoichiometry	1.05 (fuel rich)
Seed	Potassium hydroxide (KOH)
Potassium mass fraction in reactants	2.1 %
Total flow rate	54.4 g/s
Reynolds number based on hydraulic diameter	1.3×10^4
Calculated core conditions at nozzle exit	
Velocity	174 m/s
Temperature	2750 K
Mass density	0.122 kg/m^3
Mach number	0.17
Electrical conductivity	14 S/m
Electron mobility	0.37 m^2/V·s
Channel conditions	
Wall temperatures	
Insulator (estimated)	1900 K
Electrodes	1000 K
Magnetic induction	2.4 T
Electron Hall parameter	0.8
Applied Hall current	9.3 A
Magnetic interaction parameter at velocity measurement plane, based on applied Hall current	1.1

TABLE 2. Run conditions.

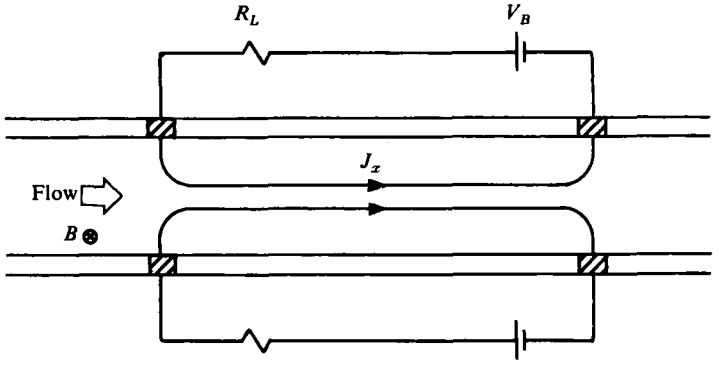

FIGURE 5. Electrical configuration for driving Hall current.

to the axial inertia of the flow. The value of S in the present experiments was about 1.1 at the plane of the velocity measurements and slightly less at the measurement planes for conductivity and electrode temperature. This value is comparable to a similarly defined value based on the Hall current density in the core of a commercial-scale channel.

3.3. *Laser-Doppler anemometry system*

Plasma velocities were measured using laser-Doppler anemometry. The LDA system, shown schematically in figure 6, used a dual-beam single-colour backscatter configuration. The optical train consisted primarily of TSI modular components. Measurements of the x- and y-directed velocity components were made separately

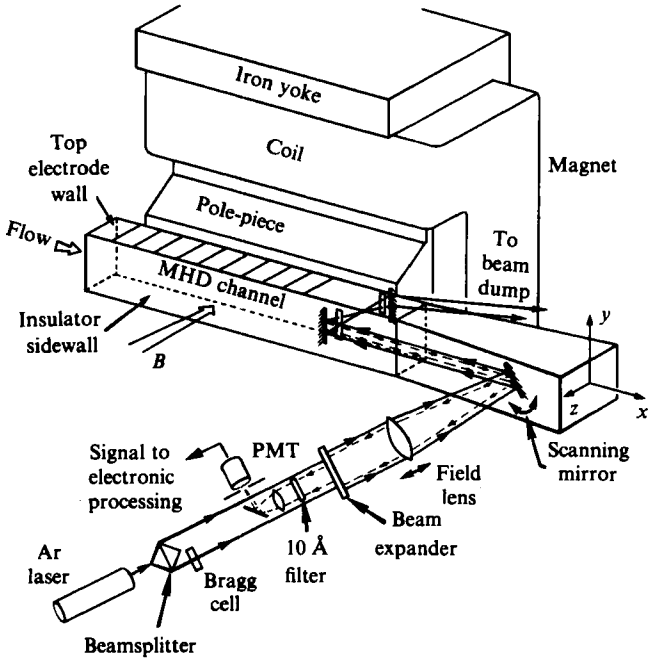

FIGURE 6. Laser-Doppler anemometry system.

by rotating components of the optical train by 90°. For the y-directed measurements a Bragg cell was used to frequency shift one of the transmitted beams by 40 MHz so as to allow discrimination of positive and negative velocities. Tight spatial and spectral filtering was used to maximize the signal-to-noise ratio of the collected scattered light; this included a narrow-line (10 Å half-width) interference filter, the purpose of which was to filter the highly radiative background emanating from the hot potassium-laden plasma.

Suitable light-scattering centres were obtained by seeding the fuel with zirconia particles having a mean diameter of 0.7 μm. These were mixed into an ethanol–glycerine slurry and then injected into the fuel line by means of a mechanical injector utilizing a slowly descending piston. Optical access to the plasma was provided by an open slit cut into the channel sidewall and located at the leading edge of the downstream electrodes.

The photomultiplier tube signal was processed by a TSI 1990A counter-type processor interfaced to an HP-21MX laboratory computer. Typical data rates were ~500 Hz; total sample size was chosen in each case so that the sampling interval was about one minute.

The major sources of experimental uncertainty in these measurements were the imperfect stationarity in conditions (including combustion temperature and applied current) and the difficulty in perfectly aligning the intersecting beams for the transverse velocity measurements. The latter problem is always important in secondary flow measurements, because a slight misalignment introduces a portion of the much higher axial velocity into the transverse velocity measurement (see Melling & Whitelaw (1976) for a brief review of this question in relation to secondary-flow measurements made by hot-wire anemometry as well as by LDA). In the present experiments the problem was exacerbated by the fact that turning the magnet on

or off caused a slight shift of the entire channel; a calibration procedure was devised to correct for the effect of this occurrence on the measured transverse velocities. A detailed uncertainty analysis by Girshick (1985) estimated the cumulative uncertainty (to 10:1 confidence) in the mean velocity measurements as ± 0.016 for $\bar{v}/U_b$ in the MHD cases and ± 0.0055 in the non-MHD case, and ± 0.045 for $\bar{u}/U_b$, where $\bar{v}$ and $\bar{u}$ are respectively the y- and x-directed components of the mean velocity. The uncertainty in spatial location was estimated as ± 0.011 for y/H, ± 0.031 for z/W in the measurements of secondary flow and ± 0.042 for z/W in the measurements of axial velocity, where H and W are respectively the channel height and width. The major contributions to this uncertainty were the finite size of the measurement volume and the uncertainty in locating the wall.

3.4. *Conductivity measurements*

The effect of secondary flow on the plasma conductivity profile was investigated by driving a Faraday discharge across a set of electrodes whose external circuitry was separate from that used to drive the Hall current. This set consisted of three electrode pairs located just upstream of the optical port. These electrodes were used only for the conductivity measurements, and were open-circuited at all other times. Near-electrode voltage drops in both the x- and y-directions were obtained from a grid of iridium voltage pins inserted through a channel sidewall. Voltage distributions were obtained over a range of values for J_y, and under various applied conditions, including:

(i) applied Faraday current only;
(ii) both Faraday current and Hall current;
(iii) Faraday current with magnetic field; and
(iv) Faraday current, Hall current and magnetic field.

For cases (iii) and (iv) measurements were made with the magnetic field pointing in both the positive- and negative-z directions. The open-circuit voltage with magnetic field was measured as well. Note that only case (iv) would be expected to drive secondary flow.

The voltage information was analysed using an approximate model based on the expression, obtainable from the generalized Ohm's law,

$$\bar{\rho} = \frac{\overline{E_y} - \overline{uB} + \beta \overline{E_x}}{(1+\beta^2) J_y}, \tag{7}$$

where ρ is the resistivity, E_y and E_x the electric-field components and u the axial velocity. The overbar indicates an average over a region of the cross-plane that encompasses the width W in the z-direction and ranges in the y-direction from the electrode surface to the height of the nearest voltage pin, a distance of 6.2 mm, or $\frac{1}{8}H$, H being the channel height. The major assumptions of the model are: that the transverse conductivity distribution in the absence of secondary flow is symmetric; that the near-electrode voltage gradients are much greater in the y-direction than in the z-direction; that the term J_y in the denominator of (7) is constant, and can be estimated using a 'current-constriction factor' obtained from a comparison of the data from cases (i) and (iii) in the above list; and that β is constant. The data from the first case were also used to estimate a constant value for the cathode surface-sheath voltage drop, which was subtracted from the measured value of E_y for the near-cathode data.

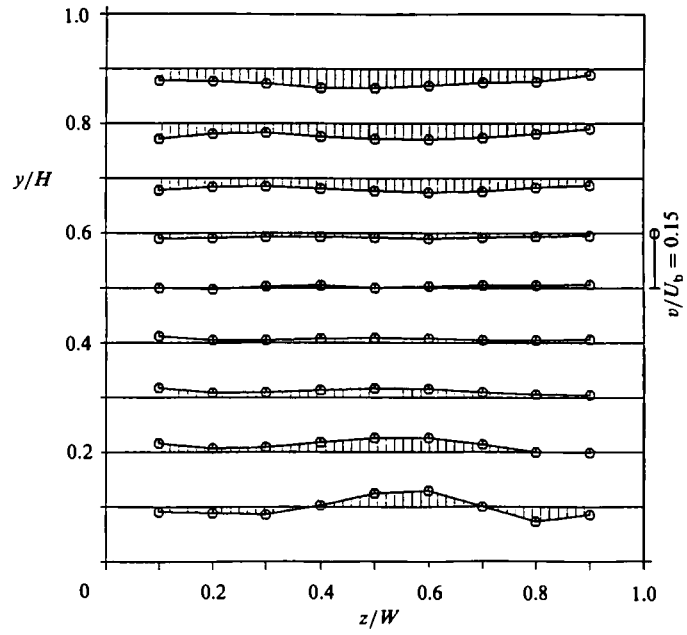

FIGURE 7. Measurements of the mean y-directed velocity (normalized by U_b) without magnetic field. ⊙, data points.

3.5. *Temperature measurements*

All electrodes were fitted with thermocouples located close to their surfaces. Of particular interest were the temperatures of the electrode pair just upstream of the velocity measurement plane, for cases in which these electrodes were not passing current. A number of measurements were recorded in which a case without secondary flow (i.e. without the simultaneous presence of magnetic field and Hall current) was immediately followed or preceded by a case with secondary flow (i.e. both were present). The change in surface temperature between these two cases could then be attributed to altered heat transfer as a result of secondary flow. As with the other measurements, data were collected for both the positive- and negative-z orientations of the magnetic induction.

4. Experimental results

4.1. *Transverse velocity measurements*

Non-MHD case

So as to have a base case with which to compare the measurements with MHD effects present, measurements of the y-directed velocity were made for the case of zero magnetic induction and zero current. The results are shown in figure 7. The peak measured transverse velocity was $0.05U_b$. This is significantly higher than reported measurements for secondary flows driven purely by the interaction of turbulence stresses with the corners of a rectangular duct. Several factors may be involved in this discrepancy, including combustion non-uniformities and other non-idealities related to the combustor, density gradients, and the heterogeneous nature of the channel walls (the top and bottom walls had alternating sections of brick and of electrodes, whereas the sidewalls had only brick).

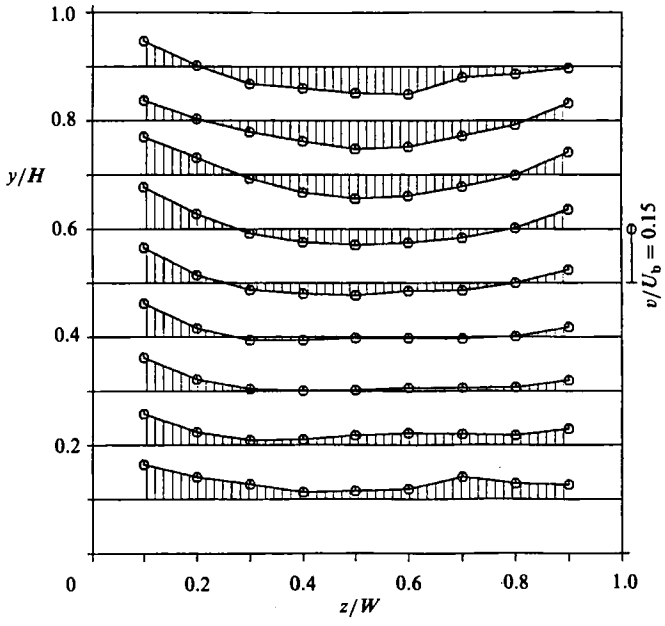

FIGURE 8. Measurements of the mean y-directed velocity (normalized by U_b) with the magnetic field pointing in the positive-z direction. ⊙, data points.

The data appear to indicate a top–bottom asymmetry, in that flow toward the corners appears at the bottom of the cross-plane but not at the top. This may possibly be ascribable to top–bottom density non-uniformity from the combustor. It is also possible that flow toward the top corners would have been observed had measurements been made closer to these corners.

MHD cases

Measurements of the y-directed velocity were made for the complete set of conditions listed in table 2, and with the magnetic field pointing in both the positive- and negative-z directions. Reversing the magnet polarity reverses the sign of the Lorentz force, and so should be approximately equivalent to rotating the channel by 180° about its axis.

The measurements for the case of $\boldsymbol{B}$ pointing in the positive-z direction are shown in figure 8. In this figure and in the figures following the secondary flow appears stronger near the left sidewall than near the right; we believe that this is an artefact caused by a consistently erroneous measurement of the wall location. Shifting all the measurement locations to the left by an amount $\Delta(z/W) = 0.035$ would produce a symmetric result, which is physically what we would expect. This systematic error is additional to the uncertainty in spatial location discussed above.

In any case, the results suggest the presence of two large counter-rotating secondary flow cells, with the flow in the core directed downward in agreement with the first-order argument illustrated in figure 2. The peak measured velocities, found in the sidewall region, measured $0.12U_b$; as the magnitude of the transverse velocity was increasing steeply towards the sidewall, it is reasonable to assume that significantly higher velocities would have been found had measurements been made closer to the walls.

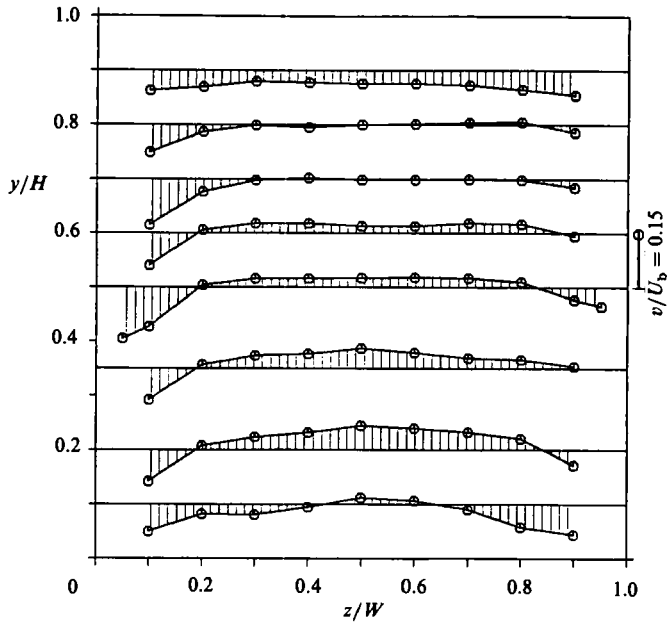

FIGURE 9. Measurements of the mean y-directed velocity (normalized by U_b) with the magnetic field pointing in the negative-z direction. ⏀, data points.

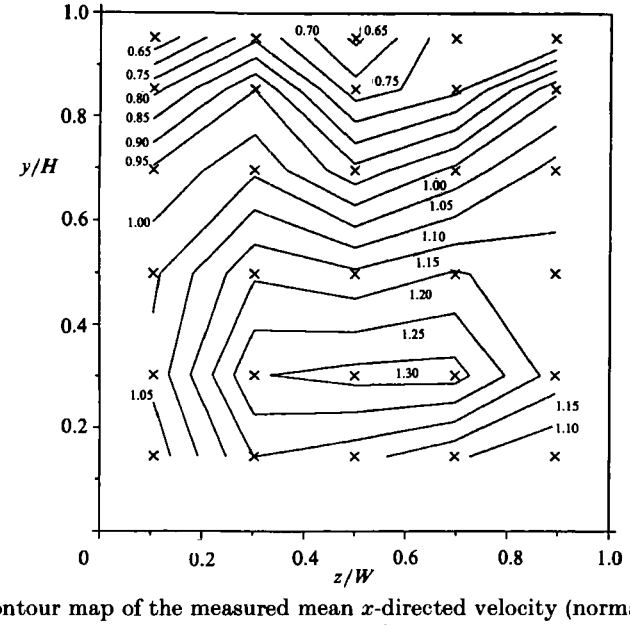

FIGURE 10. Contour map of the measured mean x-directed velocity (normalized by U_b) with the magnetic field pointing in the positive-z direction. ×, measurement locations.

The vorticity is concentrated in the top half of the channel, with the vortex cells closing at about $y/H = 0.35$. An explanation for this behaviour is suggested by a three-dimensional numerical simulation performed by Maxwell, Early & Demetriades (1985) for conditions that were similar to those of the present experiments. In these calculations the secondary-flow field at the upstream end of the interaction region

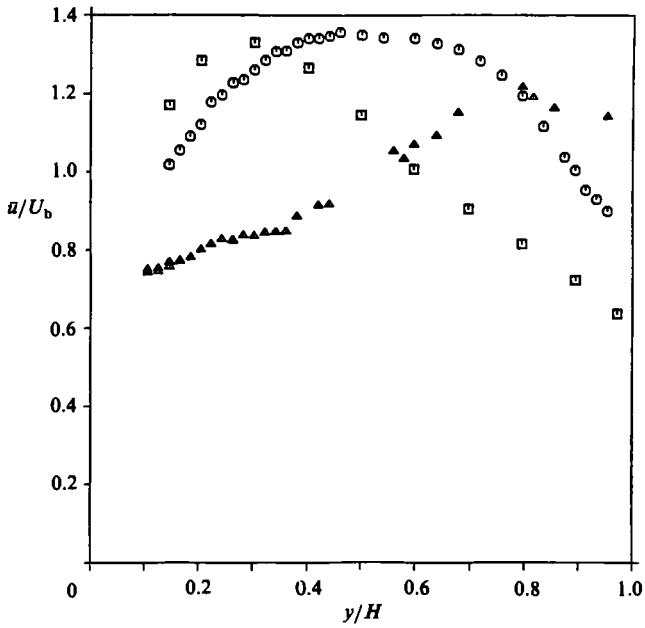

FIGURE 11. Measurements of the mean x-directed velocity along the z-centreline, for three conditions of the transverse Lorentz force F_y. □, $F_y < 0$; ○, $F_y = 0$; △, $F_y > 0$.

has a symmetric structure similar to that in figure 2. As the flow progresses, hot plasma from the core has time to be swept sideways and then upwards as it follows a secondary-flow path. This has the effect of increasing $\partial J_x/\partial z$ in the upper sidewall regions, which in turn intensifies the vorticity in these regions. The coupling between $\partial J_x/\partial z$ and axial vorticity causes the secondary-flow cells to migrate toward the top walls in the downstream half of the channel. In this respect the simulation and the measurements are in good agreement. The quantitative agreement is also reasonably good, although precise comparisons would require a more detailed specification than is available of the sidewall temperature distributions and of the upstream turbulence history. Both of these factors were shown in the simulation to have a substantial influence on the secondary flow field: the sidewall temperature because it affects $\partial J_x/\partial z$; the turbulence intensity because of its cross-plane smoothing effect.

The measurements in the region at the bottom of the cross-plane indicate a flow that was everywhere directed away from the bottom wall. A possible explanation for these measurements is discussed in connection with the temperature results.

In figure 9 the results for the case with the magnet polarity reversed are shown. As anticipated, the velocity field was upside-down compared with the results in figure 8. A few measurements were made in this case closer to the sidewalls, resulting in a peak transverse velocity measurement of $0.15U_b$.

4.2. *Effects of secondary flow*

The measured secondary-flow field was certainly strong enough to have an effect on several aspects of the plasma momentum and thermal behaviour. This subsection reports the results of the measurements of mean axial velocity, turbulence intensity, electrical conductivity and electrode surface temperature.

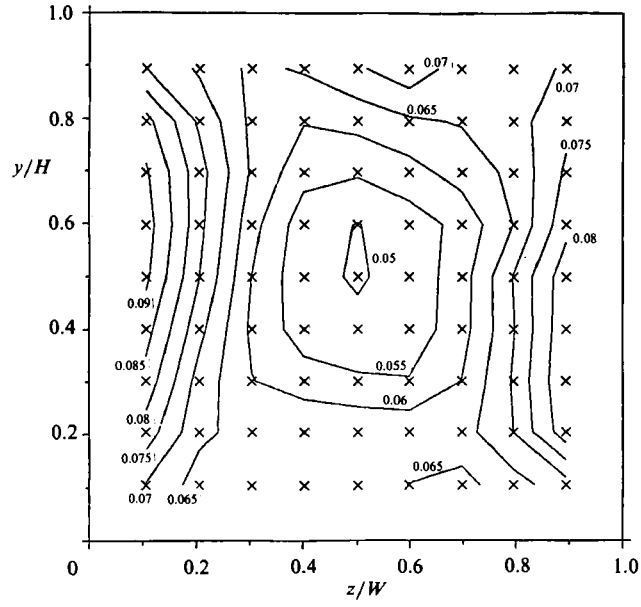

FIGURE 12. Contour map of the measured y-directed turbulence intensity (normalized by U_b) without magnetic field. ×, measurement locations.

Mean axial velocity

Measurements of the mean axial velocity with the magnetic field pointing in the positive-z direction are shown in figure 10; these results correspond to the secondary flow field shown in figure 8. The distortion of the velocity profile was dramatic: the peak velocity was forced downward from the centre of the cross-plane to a position of about $y/H = 0.3$. The isovels near the top wall follow the vortex pattern, as slow-moving fluid was swept upward along the sidewall and then pushed downward along the z-centreline. The axial velocity profiles along the z-centreline for three conditions of the magnetic field are shown in figure 11. As expected the profile was symmetric when Lorentz forces were absent; with Lorentz forces present the profile became strongly skewed according to the direction of the force.

These results are similar to the measurements reported by McClaine *et al.* (1985). In their experiments, performed in the larger Avco Mk VI channel, the conditions included a magnetic induction of 4 T, an interaction length of 2.5 m, and peak velocities of about 1000 m/s. Unfortunately the electrical loading that was used during these particular measurements was not reported; their tests encompassed a wide range of loading conditions in both Faraday and diagonal configurations.

While the axial-velocity profiles measured in the present experiments were strongly skewed, there was no evidence of the occurrence of a magnetoaerothermal instability. This is not remarkable in view of the fact that the experiments were designed to suppress the Faraday current while imposing a Hall current. In the magnetoaerothermal case the Hall current is driven by the conductivity non-uniformity encountered by the Faraday current; this non-uniformity is then amplified by secondary flows driven by the Hall current (Demetriades *et al.* 1981). In the present experiments the local Hall current is still coupled to secondary flow, but the regulation of the total Hall current may have precluded the emergence of an instability.

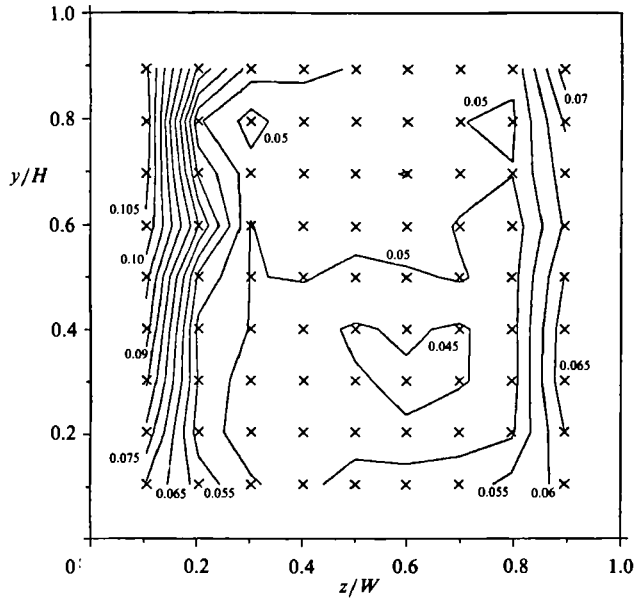

FIGURE 13. Contour map of the measured y-directed turbulence intensity (normalized by U_b) with the magnetic field pointing in the positive-z direction. ×, measurement locations.

Turbulence intensity

Previous measurements of turbulence intensity in the Stanford M-2 channel have found relatively high values of the centrepoint axial turbulence intensity $\tilde{u}_c/\overline{u}_c$, where $\tilde{u}_c$ is the turbulence velocity (the standard deviation of the velocity probability distribution function) and $\overline{u}_c$ is the centrepoint mean velocity. For example, Reis & Kruger (1986) measured values ranging from 6.6 % to 9.6 % for a variety of non-MHD flow cases; in the present experiments several measurements of $\tilde{u}_c/\overline{u}_c$ yielded values ranging from 5.8 % to 6.3 %. For comparison, Melling & Whitelaw (1976) in their water-flow experiment measured values of 4–5 % at an axial location where the boundary layers had merged. It has been conjectured that the relatively high axial turbulence in the Stanford channel is caused by combustion non-uniformities. The measured value in the non-MHD case of the y-directed core turbulence $\tilde{v}$, again normalized by $\overline{u}_c$, was 3.75 %; this is virtually identical with the value reported by Melling & Whitelaw.

Measurements of the y-directed turbulence intensity in the non-MHD case are shown in figure 12, in which the measured values of $\tilde{v}$ have been normalized by U_b. As expected the distribution was symmetric and $|\tilde{v}|$ was greater near walls parallel to y than near walls normal to y.

The measurements made in the MHD case, with the magnetic field pointing in the positive-z direction, are shown in figure 13. The region of minimum turbulence (whose magnitude was somewhat less than in the non-MHD case because of turbulence damping by the magnetic field; cf. Reis & Kruger 1986) was shifted downward by Lorentz forces.

The measurements for $\tilde{u}/U_b$, shown in figure 14, exhibited the same effect; these same measurements are shown in figure 15 normalized instead by the local mean velocity $\overline{u}$. In these measurements there appears to be a region beneath the centre of the top wall where the turbulence was greater than its value closer to the wall; this might be explainable in terms of secondary-flow convection.

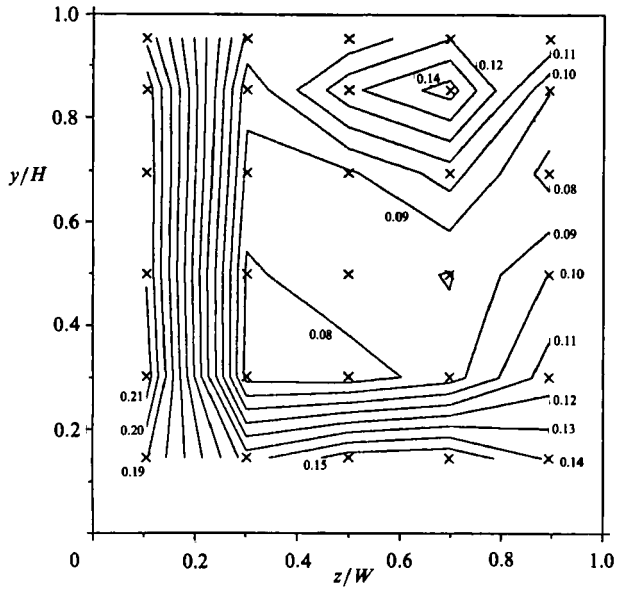

FIGURE 14. Contour map of the measured x-directed turbulence intensity (normalized by U_b) with the magnetic field pointing in the positive-z direction. ×, measurement locations.

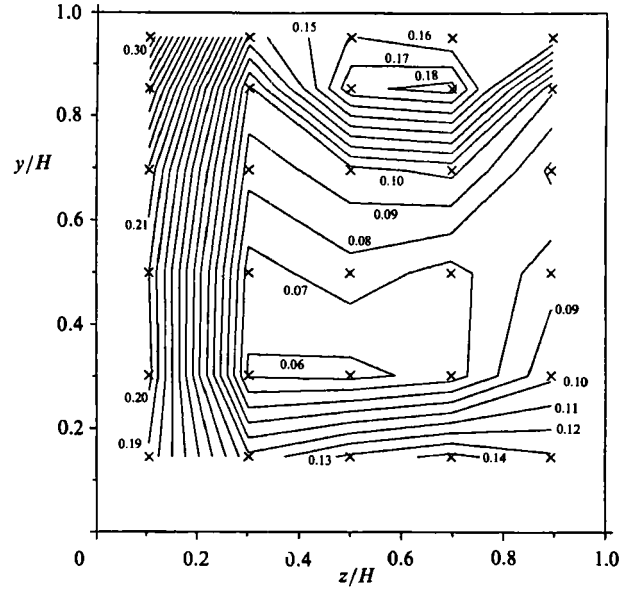

FIGURE 15. Contour map of the measured x-directed turbulence intensity (normalized by the local mean axial velocity) with the magnetic field pointing in the positive-z direction. ×, measurement locations.

Electrical conductivity

The results of the conductivity measurements for the MHD cases are summarized in figure 16, in which the near-electrode resistivity defined by (7) has been normalized by the value of the core conductivity measured without magnetic field. The terms 'anode region' and 'cathode region' refer respectively to the regions adjacent to the

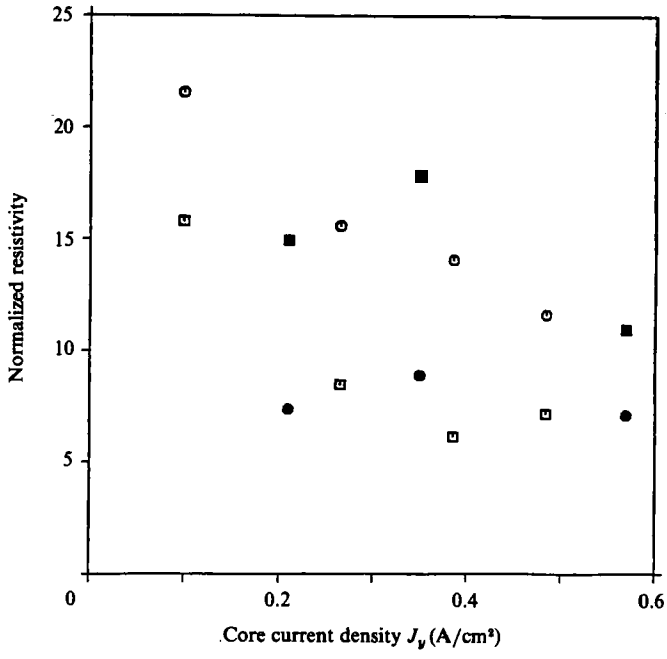

FIGURE 16. Average resistivity in near-electrode regions (normalized by the core resistivity measured without magnetic field) for cases with the complete electrical configuration and magnetic field. Anode region: ⊡, $B < 0$; ■, $B > 0$. Cathode region: ⊙, $B < 0$; ●, $B > 0$.

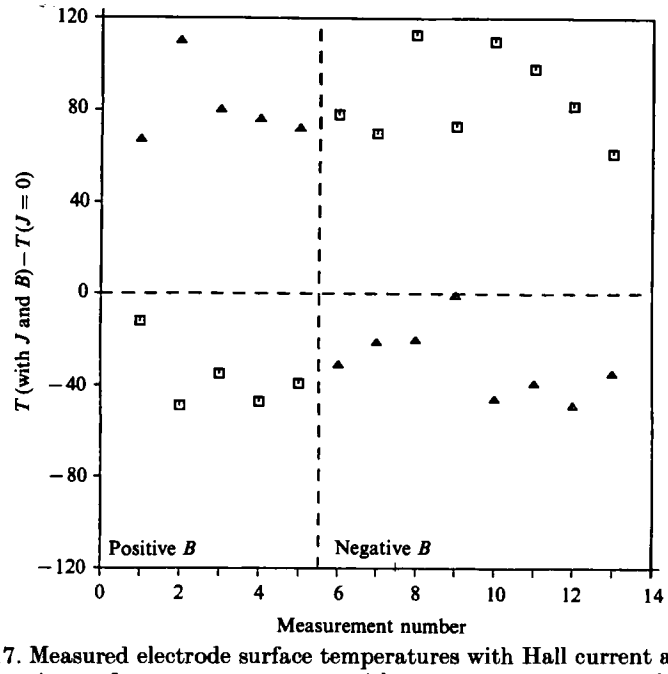

FIGURE 17. Measured electrode surface temperatures with Hall current and magnetic field minus reference measurements without current. ⊡, top; △, bottom.

top and bottom electrodes that were used for the conductivity measurements. The abscissa in this figure represents the value of the core current density associated with the Faraday discharge; for all the data shown the Hall circuit was active as well, corresponding to case (iv) in §3.4.

The decrease in resistivity as J_y increased was an expected consequence of Joule heating. Otherwise these results indicate that secondary flow caused the resistivity distribution to become significantly asymmetric. The boundary layer receiving cold sidewall fluid was much more resistive than the boundary layer toward which hot core fluid was directed; the average value of the ratio of the higher resistivity to the value at the opposite wall was 1.8. The importance of these results is that near-electrode voltage drops, which are a performance-limiting effect in combustion MHD devices, can be significantly altered by secondary flow.

Electrode surface temperatures

Thirteen separate measurements were made of the effect of secondary flow on electrode surface temperatures, as described above in §3.5. The results are shown in figure 17. Each point in this figure represents the temperature with secondary flow (with simultaneous Hall current and magnetic field) minus the temperature without secondary flow (without current); the latter temperature was typically about 1000 K. A separate analysis of data not shown in the figure indicates that the presence of magnetic field alone made no difference in the temperature, while the presence of Hall current alone caused a warming of both the top and bottom electrodes by an average of about 10 K, because of Joule heating.

The effect of secondary flow in the positive-B case is seen to be a substantial heating of the bottom electrode and a smaller but still significant cooling of the top electrode; reversing the magnet polarity reversed the results. The electrode toward which hot core fluid was pushed was heated on the average by 85 K; the opposite electrode was cooled by an average of 32 K. Using the fact that the electrodes were cooled by water at about 300 K, we calculate that secondary flow evidently caused a 12% increase in the heat flux from the plasma to the heated electrode and a 5% reduction in the heat flux to the cooled electrode.

Aside from the obvious conclusion that secondary flow has the expected qualitative asymmetric effect on heat transfer to the top and bottom walls, it is interesting to consider the surprising result that the effect at the heated electrode was more than twice as great as the effect at the cooled electrode. This result is surprising: first because the secondary flow cells appeared to be concentrated near the cooled electrode, and secondly because the resistivity measurements showed the opposite trend, with a stronger effect being observed in the region adjacent to the cooled electrode.

A possible explanation is as follows. As already noted, the secondary-flow cells not only sweep cold sidewall fluid into the top-wall boundary layer, but also eventually convect hot core fluid around a loop into the same boundary layer in the sidewall region. As the stainless-steel electrodes are thermally quite conductive, the net result is that the cooling effect is mitigated; no such effect occurs for the boundary layer of the bottom wall, toward which core fluid has been pushed but which has less vortical mixing. Distortion of the turbulence distribution could also be a factor in the asymmetrical heat transfer. Near-electrode voltage drops, on the other hand, are dependent on complex physical processes which are strongly but nonlinearly temperature-dependent. Since the calculated resistivities were averaged over an area described in §3.4, it is not remarkable that the net quantitative effects for the

resistivity distribution could be quite different than for heat transfer, although the qualitative trends were the same.

The temperature results suggest a possible explanation for the secondary flow measurements in the region near the bottom wall (in the positive-B case). The substantial warming of the bottom electrode suggests that the mass density near the bottom wall may have been decreasing in the axial direction, causing a net reduction in the axial mass flux which would have to be balanced by a flow away from the wall. Flow away from the bottom wall did not appear in the simulation of Maxwell *et al.* (1985). However, their calculations assumed a constant wall temperature. It is possible that such a flow effect might appear in the simulations if the wall temperature were coupled to the flow field.

5. Summary and conclusions

Experiments were conducted to measure MHD-induced secondary flow. The results constitute the first direct, quantitative measurements of secondary flow in a combustion MHD channel. The experiments were performed in a laboratory channel, with dimensions an order of magnitude smaller than in envisoned full-scale MHD devices; however, the use of an applied Hall current and of a relatively low axial velocity resulted in a value for the magnetic interaction parameter based on the Hall current of 1.1, which is comparable to anticipated values in the core of a commercial-scale MHD generator.

Laser-Doppler anemometry measurements of transverse velocities under various controlled conditions showed that Lorentz forces caused large-scale secondary flows to develop over a downstream channel cross-plane. Peak measured transverse velocities were as high as 15% of the bulk velocity. The structure of the measured secondary-flow field was qualitatively in accord with simple models, with a concentration of the vortices toward the top wall explainable in terms of the coupling between axial vorticity and non-uniformities in the Hall current density.

Several effects of MHD secondary flow were also investigated, including the skewing of the cross-plane distributions of mean axial velocity and of the axial and transverse components of turbulence intensity, and the development of asymmetries in the wall heat flux and in the near-electrode conductivity. These results consistently demonstrated that secondary flow exerted a profound influence on the plasma momentum, thermal and electrical behaviour. The major conclusion is that secondary flow is an important effect which needs to be accurately assessed in designing full-scale MHD devices.

REFERENCES

APOLLONSKII, S. M. & KOS'KIN, YU. P. 1968 On transverse velocity disturbances in magnetohydrodynamic channel flows. *Magnetohydrodynamics* **4**, 37.

BARTON, J. P. 1980 Fluctuations in combustion driven MHD generators. Ph.D. dissertation; *HTGL Report* 118, *Stanford University*.

BITYURIN, V. A., ZATELEPIN, V. N. & LYUBIMOV, G. A. 1978 Effect of force field nonuniformity on flow in an MHD channel. *Fluid Dyn.* **13**, 1.

BROER, L. J. F., PELETIER, L. A. & WIJNGAARDEN, L. VAN 1960 A mechanical Hall effect. *Appl. Sci. Res.* B, **8**, 259.

DEMETRIADES, S. T., MAXWELL, C. D. & OLIVER, D. A. 1983 Progress in analytical modeling of MHD power generators II. In *Proc. 21st Symp. on Engineering Aspects of Magnetohydrodynamics, Argonne, Illinois.*

DEMETRIADES, S. T., OLIVER, D. A., SWEAN, T. F. & MAXWELL, C. D. 1981 On the magneto-aerothermal instability. *AIAA 19th Aerospace Sciences Meeting, St Louis, Paper* AIAA-81-0248.

DOSS, E. D. & AHLUWALIA, R. K. 1983 Three-dimensional flow development in MHD generators at part load. *J. Energy* **7**, 289.

FAY, J. A. 1959 Hall effects in a laminar boundary layer of the Hartmann type. *Avco-Everett Research Report* 81.

GIRSHICK, S. L. 1985 Secondary flow in a magnetohydrodynamic channel. Ph.D. dissertation, Stanford University.

GIRSHICK, S. L. & KRUGER, C. H. 1983 Evidence of secondary flow in Faraday MHD generators. In *Proc. 21st Symp. on Engineering Aspects of Magnetohydrodynamics, Argonne, Illinois.*

ISHIKAWA, M. & UMOTO, J. 1984 New approach to calculation of three-dimensional flow in MHD generators. In *Proc. 22nd Symp. on Engineering Aspects of Magnetohydrodynamics, Starkville, Mississippi.*

JAMES, R. K. & KRUGER, C. H. 1983 Joule heating effects in the electrode wall boundary layer of MHD generators. *AIAA J.* **21**, 679.

LIU, B. L., LINEBERRY, J. T. & SCHMIDT, H. J. 1983 Simplified three-dimensional modeling for MHD DCW channels. *J. Energy* **7**, 456.

MCCLAINE, A. W., SWALLOM, D. W. & KESSLER, R. 1985 Experimental investigation of subsonic combustion-driven MHD generator performance. *J. Propulsion* **1**, 263.

MAXWELL, C. D., EARLY, D. W. & DEMETRIADES, S. T. 1985 Predicted strength and influence of MHD-induced secondary flows in recent experiments. In *Proc. 23rd Symp. on Engineering Aspects of Magnetohydrodynamics, Somerset, Pennsylvania.*

MAXWELL, C. D., MARKHAM, D. M., DEMETRIADES, S. T. & OLIVER, D. A. 1977 Coupled electrical and fluid calculations in the cross-plane in linear MHD generators. In *Proc. 16th Symp. on Engineering Aspects of Magnetohydrodynamics, Pittsburgh.*

MELLING, A. & WHITELAW, J. H. 1976 Turbulent flow in a rectangular duct. *J. Fluid Mech.* **78**, 289.

MITCHNER, M. & KRUGER, C. H. 1973 *Partially Ionized Gases.* Wiley.

REIS, J. C. & KRUGER, C. H. 1986 Turbulence suppression in combustion-driven magnetohydrodynamic channels. *J. Fluid Mech.* (accepted for publication).

SASTRY, V. U. K. & BHADRAM, C. V. V. 1978 Effect of Hall currents on the hydromagnetic flow in an annular channel with a radial magnetic field. *Phys. Fluids* **21**, 857.

SATO, H. 1961 The Hall effect in the viscous flow of ionized gas between parallel plates under transverse magnetic field. *J. Phys. Soc. Japan* **16**, 1427.

STARR, R. F., CHRISTENSEN, L. S., GARRISON, G. W. & WHITEHEAD, G. L. 1982 Preliminary Faraday performance of a large magnetohydrodynamic generator at high magnetic field. *J. Energy* **6**, 163.

SWEAN, T. F., OLIVER, D. A., MAXWELL, C. D. & DEMETRIADES, S. T. 1981 Prediction of transverse asymmetries in MHD ducts with zero net Hall current. *AIAA J.* **19**, 651.

TANI, I. 1962 Steady flow of conducting fluids in channels under transverse magnetic fields, with consideration of Hall effect. *J. Aerosp. Sci.* **29**, 297.